Axisymmetric Cavity Flows Past Slender Bodies of Revolution

Y. S. Chou*
Lockheed Palo Alto Research Laboratory, Palo Alto, Calif.

Axisymmetric cavity flows past slender bodies of revolution have been solved by distributing singularities on the body-cavity axis and by invoking the slender body approximation. Solutions are presented for a 5-degree cone and for a blunt cone-cylinder. In the case of a cone, solutions are compared with either experimental data or with available exact solutions. Agreements are found to be good. The effects of gravity and cavity pressure on both the cavity shape and the pressure distribution are shown.

Nomenclature

B = normalized body-cavity length
C_D = drag coefficient
C_p = pressure coefficient
d_{max} = maximum cavity diameter
F = Froude number, defined by Eq. (8)
g = gravitational acceleration
L = body length
l = cavity length
m = source strength
P = pressure
P_∞ = freestream pressure
q^2 = total speed defined by Eq. (7)
$R_b(x)$ = body shape
$R_c(x)$ = cavity shape
R_m = maximum radius of body-cavity system
r = perpendicular distance from axis of symmetry
u = perturbation velocity component in the x direction
U_∞ = freestream velocity
v = perturbation velocity component in the r direction
Φ = velocity potential
φ = perturbation velocity potential
δ = slenderness of body-cavity system, defined as Rm/B
ρ = density
θ = half-cone angle
σ = cavitation number defined by Eq. (8)

Introduction

THE development of underwater missiles has focused attention on the hydrodynamic characteristics of high-speed flows. One characteristic is that long trailing cavities are produced as a result of air ventilation or cavitation. The cavities in these supercavitating flows may affect a missile's hydrodynamic characteristics and flight trajectory. For this reason, the force data for supercavitating flow about a missile's body of revolution are important input parameters to the computation of underwater missile motion. The purpose of the present study is to provide solutions for axisymmetric, steady, supercavitating flow about a slender body of revolution.

Due to the successful application of the hodograph method, a great amount of work has been done for the two-dimensional cavity flow such as flows about structs and hydrofoils. The powerful hodograph method, however, ceases to be effective in the three-dimensional or axisymmetric cases. Consequently, considerable effort has been expended in seeking useful approximations for axisymmetric cavity flow.[1] But all the approximations have the common failings of involving complex numerical calculations and limited ranges of applicability. Recently Brennen[2] presented numerical solutions for the cavities behind a disk and a sphere in different sizes of a solid wall tunnel by an elaborate relaxation method. To extend this method to compute different forebody shapes in an unbounded medium seems to be numerically prohibitive. In an early report of Cuthbert and Street,[3] supercavitating flow about slender bodies of revolution was treated. Singularities (source and sink) were distributed on the body axis for the potential flow solution and a modified Riabouchinsky model was employed for the cavity closure. Because of the slenderness of the forebody, as well as the cavity, the source or sink strength is related to the local rate of change of body (or cavity) area. Therefore, they obtained a nonlinear integral differential equation for the unknown cavity shape. Their attempts in solving the integral differential equation were not entirely successful; only a few solutions for 5° and 10° cones were obtained.

A more exact solution for axisymmetric bodies has been recently given by Struck.[4] In his treatment he distributed singularities on the body and cavity surface. Solutions were obtained by first guessing a cavity position. This guessed position was then iterated upon until the constant pressure condition was satisfied on the cavity surface.

In the present study we will employ the same approach as that presented in Ref. 3, namely, we will distribute singularities on a body-cavity axis and apply a slender body theory to determine the strength of the singularities. At the cavity closure, a rear stagnation point is assumed in order to be consistent with the slender body theory. Again, a nonlinear integral differential equation is obtained for the cavity shape. This equation is reduced to a matrix equation which is solved by an iterative process. In order to obtained an initial trial solution to start the iteration, an approximate solution to the integral differential equation is obtained by reducing the equation to a pure differential one. This approximate solution is proved to be an effective initial trial solution. A few iterations upon this solution lead to a converged solution to the integral equation.

Solutions are presented in this report for a cone and for a blunt cone-cylinder. The cone solutions are compared with those given in Ref. 3 as well as with available experimental data. Agreements are found to be good. Gravity effects on both the cavity shape and pressure distribution are shown.

Because of the slender body assumption, the cavitation number is limited to the order of $\delta^2 \ln\delta$, and the Froude number has to be order of $1/\delta(\ln\delta)^{1/2}$, where δ is the slenderness parameter defined as the ratio of the maximum diameter of the body-cavity system to the length of the body-cavity system.

Received April 5, 1973; revision received August 6, 1973.
Index categories: Fluid Dynamics; Hydrodynamics.
*Research Scientist. Member AIAA.

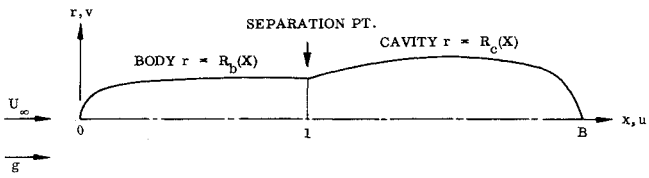

Fig. 1 Sketch of geometry.

Mathematical Development

Governing Equations

Let us choose a cylindrical coordinate system (x,r) with x along the body-cavity axis and r perpendicular to x. The origin of this coordinate system is located at the body nose. A sketch of this system is given in Fig. 1. Due to the fact that both the body and the cavity are axisymmetric, the flow field will be a function of x and r only. We will denote the body length by L; the freestream velocity by u_∞; and the free stream pressure by p_∞. Let us now normalize all length x,r by L, all velocity u,v by u_∞, and velocity potential by $u_\infty L$. Then, for the present potential flow, the normalized velocity potential can be written as:

$$\Phi = x + \varphi \tag{1}$$

where φ is the perturbation velocity potential such that the perturbation velocity components u and v are

$$u = \partial\varphi/\partial x \quad v = \partial\varphi/\partial r \tag{2}$$

By distributing singularities on the axis x, the perturbation potential function can be written as

$$\varphi = -\frac{1}{4\pi}\int_0^B \frac{m(\xi)d\xi}{[(x-\xi)^2 + r^2]^{1/2}} \tag{3}$$

where $m(x)$ is the unknown strength and B is the yet unknown body-cavity length. We note that due to the present normalization the body length is unity. Assuming the body-cavity is given by $r = R(x)$, $R(x) = R_b(x)$ is the given body and $R = R_c(x)$ is the cavity yet to be computated. It is assumed that the cavity starts at $x = 1$, then at this point

$$R_b(1) = R_c(1) \text{ and } dR_b(1)/dx = dR_c(1)/dx$$

Let us define $\delta = Rm/B$ where Rm is the maximum of $R(x)$. If $\delta \ll 1$, we can apply the well known slender body theory to determine $m(x)$. According to this theory (Ref. 5, for example), we have

$$m(x) = \pi dR^2/dx \tag{4}$$

and

$$v \simeq dR/dx$$

Consequently, we obtain

$$u = \frac{\partial\varphi}{\partial x} = \frac{1}{4}\int_0^B \frac{dR^2/d\xi(x-\xi)d\xi}{[(x-\xi)^2 + r^2]^{3/2}} \tag{5}$$

In obtaining Eq. (4), it is assumed that $dR/dx = 0(\delta)$; for this reason we see that slender body theory must fail in the blunt nose region as well as near the cavity closure. Within the region of validity of the slender body theory it can be shown[6,7] that $u = 0(\delta^2 \ln\delta)$.

The Bernoulli equation is

$$p_\infty + (1/2)\rho u_\infty{}^2 = p + (1/2)\rho u_\infty{}^2 q^2 - \rho g L(x - x_0) \tag{6}$$

where q^2 is the total speed defined as

$$q^2 = (1+u)^2 + v^2 \simeq 1 + 2u + v^2 \tag{7}$$

g is the gravity acceleration and x_0 is the reference level for the gravity field. We will choose $x_0 = 1$. Also the gravity field is assumed to act in the positive x direction. Define the cavitation number σ and Froude number F as

$$\sigma = (p_\infty - p_c)/(1/2)\rho u_\infty{}^2, \quad F = u_\infty/(gL)^{1/2} \tag{8}$$

where p_c is the cavity pressure. It is assumed that the pressure is constant inside the cavity. On the cavity surface, the pressure must also be a constant because it is a free surface, this pressure therefore must be equal to P_c. The cavity surface is a stream surface. Hence, on the cavity surface, i.e., $1 \le x \le B$, Eq. (6) becomes

$$\sigma = 2u + v^2 - 2(x-1)/F^2 \tag{9}$$

Substituting Eqs. (4) and (5) into (9), we obtain

$$\sigma = \frac{1}{2}\int_0^B \frac{(dR^2/d\xi)(x-\xi)d\xi}{[(x-\xi)^2 + R_c{}^2]^{3/2}} + \left(\frac{dR_c{}^2}{dx}\right) - \frac{2(x-1)}{F^2} \tag{10}$$

Equation (10) is the nonlinear integral differential equation for the unknown cavity shape R_c. Both the cavitation number σ and Froude number F are given parameters. Once R_c has been determined, the pressure coefficient on the forebody, as well as the drag coefficient, can be determined as the following:

$$C_p = \frac{p_b - p_\infty}{(1/2)\rho u_\infty{}^2} = -\frac{1}{2}\int_0^B \frac{(dR^2/d\xi(x-\xi)d\xi}{[(x-\xi)^2 + R_b{}^2]^{3/2}} - \left(\frac{dR_b{}^2}{dx}\right) + \frac{2(x-1)}{F^2} \quad 0 < x \le 1 \tag{11}$$

$$C_D = \frac{1}{R_b{}^2(1)}\int_0^1 C_p \frac{dR_b{}^2}{dx}dx + \sigma \tag{12}$$

In order to apply slender body theory, we mentioned before that dR/dx must be order of δ and u must be order of $\delta^2 \ln\delta$. Therefore, from Eq. (10), we see that the cavitation number σ and $1/F^2$ must also be order of $\delta^2 \ln\delta$, otherwise the slender body theory solution will not be valid.

Method of Solution

The governing equation for the axisymmetric slender cavity shape is given by Eq. (10); the boundary conditions for R_c are: at $x = 1$, $R_c = R_b$, $dR_b/dx = dR_c/dx$ and at $x = B$, $R_c = 0$. It is the purpose of this report to present solutions to Eq. (10) for various forebody shapes and different values of σ and F.

It is convenient to define a variable Y as

$$Y = R_c{}^2 \tag{13}$$

The integral part of Eq. (10) can be integrated by part once, it yields

$$\int_0^B \frac{\frac{dR^2}{d\xi}(x-\xi)d\xi}{[(x-\xi)^2 + R_c{}^2]^{3/2}} = \frac{\left(\frac{dY}{dx}\right)_B}{[(x-B)^2 + Y]^{1/2}} - \frac{\left(\frac{dR_b{}^2}{dx}\right)_0}{[(x^2-\xi)^2 + Y]^{1/2}} - \int_0^1 \frac{\frac{d^2R_b{}^2}{d\xi^2}d\xi}{[(x-\xi)^2 + Y]^{1/2}} - \int_1^B \frac{\frac{d^2Y}{d\xi^2}d\xi}{[(x-\xi)^2 + Y]^{1/2}}$$

We will assume that the cavity closes like a cone, then $dY/dx_B = 0$. For simplicity, we will denote

$$\frac{d^2Y}{dx^2} = Y'', \quad \frac{dY}{dx} = Y', \quad \left(\frac{dR^2}{dx}\right)_0 = Y_b'(0) \text{ and}$$

$$\mathfrak{L}(x) = \int_0^1 \frac{(d^2R_b{}^2/d\xi^2)d\xi}{[(x-\xi)^2 + Y]^{1/2}}$$

Eq. (10) can therefore be written as

$$\frac{1}{2}\int_1^B \frac{Y''d\xi}{[(x-\xi)^2+Y]^{1/2}} = -\left[\sigma + \mathfrak{L}(x) + \frac{Y_b'(0)}{(x^2+Y)^{1/2}} - \frac{(Y')^2}{4Y} + \frac{2(x-1)}{F^2}\right], \quad 1 \le x \le B \tag{14}$$

To solve Eq. (14), we will choose $j+1$ discrete points between $1 \le x \le B$, let $n = 1,2,\ldots,j$ such that $x_1 = 1$, $x_{j+1} = B$, between x_n and x_{n+1}, Y is assumed to be a quadratic function in x, i.e., for $x_n \le x \le x_{n+1}$

$$Y = Y_n + a_n(x-x_n) + b_n(x-x_n)^2$$

Hence, the integral in Eq. (14) becomes a summation

$$\frac{1}{2}\int_1^B \frac{Y''d\xi}{[(x-\xi)^2+Y]^{1/2}} = -\sum_{n=1}^{j} b_n \ln \frac{x-x_{n+1}+[(x-x_{n+1})^2+Y]^{1/2}}{x-x_n+[(x-x_n)^2+Y]^{1/2}} \tag{15}$$

Substituting Eq. (15) into Eq. (14), we obtain

$$\sum_{n=1}^{j} b_n \ln \frac{x-x_{n+1}+[(x-x_{n+1})^2+Y]^{1/2}}{x-x_n+[(x-x_n)^2+Y]^{1/2}} = \sigma + \mathfrak{L}(x) + \frac{Y_b'(0)}{(x^2+Y)^{1/2}} - \frac{(Y')^2}{4Y} + \frac{2(x-1)}{F^2}, \quad 1 \le x \le B \tag{16}$$

For a given x, Eq. (16) thus becomes an algebraic equation for b_n provided Y and B are known.

To determine b_n, we choose to satisfy Eq. (16) at discrete points $x = x_n$. We then obtain a matrix equation

$$\Omega_{kn}A_n = L_k \tag{17}$$

where A_n is a j-dimension vector, its component is b_n. L_k is a j-dimension vector, its component is

$$L_k = \sigma + \mathfrak{L}(x_k) + \frac{Y_b'(0)}{(x_k^2+Y_k)^{1/2}} - \frac{(Y_k')^2}{4Y_k} + 2\frac{(x_k-1)}{F^2} \tag{18}$$

and Ω_{kn} is a $j \times j$ matrix, its element is given by

$$\Omega_{kn} = \ln \frac{x_k - x_{n+1} + [(x_k-x_{n+1})^2 + Y_k]^{1/2}}{x_k - x_n + [(x_k-x_n)^2 + Y_k]^{1/2}} \tag{19}$$

where Y_k is Y at $x = x_k$. Y_k' is dY_k/dx at x_k. Equation (17) can be solved by a standard matrix inversion provided that Ω_{kn} and L_k can be calculated. Once b_n is determined, a_n can be calculated by requiring that dY/dx be continuous at every discrete point. We obtain

$$a_{n+1} = a_n + 2b_n(x_{n+1} - x_n) \tag{20}$$

From the boundary condition that $R_c(1) = R_b(1)$, $dR_c(1)/dx = dR_b(1)/dx$, it is clear that $a_1 = 2R_b(1)dR_b(1)/dx$.

Once a_n and b_n are known, we can compute Y_k which is given as follows:

$$Y_k = R_b^2(1) + \sum_{n=1}^{k-1}[a_n(x_{n+1}-x_n) + b_n(x_{n+1}-x_n)^2] \text{ for } x > 1$$

$$Y_k = R_b^2(1) \text{ for } x = 1 \tag{21}$$

In Eq. (21) we have used the boundary condition that at $x = 1$, $R_c^2 = R_b^2$. The body-cavity length B should be determined such that $Y = 0$ at $x = B$. In order to solve the matrix equation, Eq. (17), an initial guessed solution must be made so that proper discrete point X_k can be chosen and Ω_{kn} and L_k can be calculated. Based on this guessed solution, one can obtain the calculated solution Y_k as given by Eq. (21). If the calculated Y_k does not agree with the guessed Y_k, new guessed Y_k will be given and iteration will continue until a converged solution is obtained.

Once the cavity shape has been found, the pressure coefficient on the forebody surface can be calculated according to

$$C_p = \sum_{n=1}^{j} b_n \ln \frac{x-x_n+[(x-x_n)^2+R_b^2]^{1/2}}{x-x_{n+1}+[(x-x_{n+1})^2+R_b^2]^{1/2}} + \mathfrak{L}(x) - \left(\frac{dR_b}{dx}\right)^2 + \frac{2(x-1)}{F^2} + \frac{R_b(0)dR_b(0)/dx}{(x)^{1/2}}, \quad 0 < x \le 1 \tag{22}$$

Approximate Solution

We will now develop an approximate solution to be used as the initial guessed profile in the iteration process described above. Under the present approximation, the original integral differential equation, Eq. (10), will be reduced to a differential equation. Standard numerical methods in solving the ordinary differential equations can be employed and solutions can be easily obtained.

According to Laitone,[5] the perturbation velocity on the surface of a slender body which is given by an integral can be approximated by an infinite series of local area differentials.

$$2u = \frac{1}{2}\int_0^B \frac{(dR^2/d\xi)(x-\xi)d\xi}{[(x-\xi)^2+R^2]^{3/2}} = -\frac{1}{2}\left\{\frac{dR^2}{dx}\frac{(B-2x)}{x(B-x)} + \frac{d^2R^2}{dx^2}\left[\ln\frac{4x(B-x)}{R^2} - 2\right] + \frac{d^3R^2}{dx^3}\frac{(B-2x)}{2} + \ldots + 0(R)\right\} \tag{23}$$

Assuming $|d^3R^2/dx^3| \ll |d^2R^2/dx^2|$, we can approximate the right hand side of Eq. (23) by only two terms,

$$\frac{1}{2}\int_0^B \frac{(dR^2/d\xi)(x-\xi)d\xi}{[(x-\xi)^2+R^2]^{3/2}} \simeq -\frac{1}{2}\left\{\frac{dR^2}{dx}\frac{(B-2x)}{x(B-x)} + \frac{d^2R^2}{dx^2}\left[\ln\frac{4x(B-x)}{R^2} - 2\right]\right\} \tag{24}$$

Applying Eq. (24) on a cavity surface and substituting it into Eq. (10), we obtain an equation for cavity shape R_c as:

$$x(B-x)\left[\ln\frac{4x(B-x)}{R^2} - 2\right]\frac{d^2Y}{dx^2} = -\frac{dY}{dx}(B-2x) + 2x(B-x)\left[\frac{1}{4}\frac{\left(\frac{dY}{dx}\right)^2}{Y} - \sigma - \frac{2(x-1)}{F^2}\right], \quad 1 \le x \le B \tag{25}$$

After some manipulation, it can be shown that Eq. (25) can be reduced to the following system of first order equa-

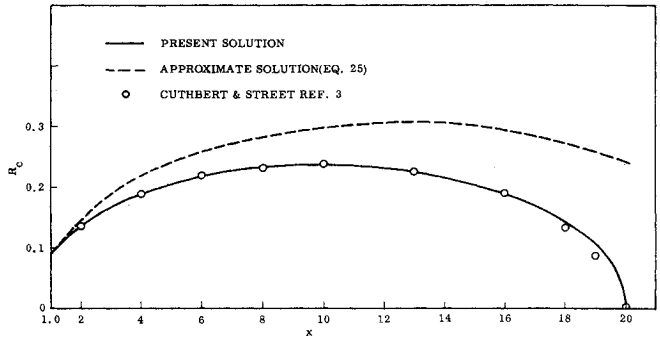

Fig. 2 Cavity shapes for a 5° cone at $\sigma = 0.0042$, $F \to \infty$.

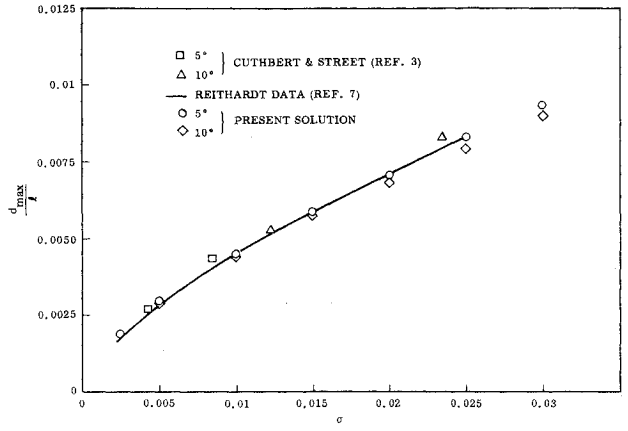

Fig. 4 Fineness ratio for cones vs cavitation number, $F \to \infty$.

tions

$$\frac{dY}{dx} = -\frac{2\left\{G + (x-1)\left(\sigma + \frac{x-1}{F^2}\right) - R_b(1)\left(\frac{dR_b}{dx}\right)_1\left[\ln\frac{4(B-1)}{R_b^2(1)} - 2\right]\right\}}{\ln\frac{4x(B-x)}{Y} - 2} \tag{26}$$

$$\frac{dG}{dx} = \frac{(dY/dx)^2}{4Y}$$

Equation (26) is an initial value problem provided B is given. The initial conditions are, at $x = 1$, $Y = R_b^2(1)$, $G = 0$, $(dY/dx) = 2R_b(1)dR_b/dx)_1$. The unknown parameter B is determined by the condition that $Y = 0$ at $x = B$.

To solve Eq. (26), a guessed value for B has to be made. This value is then iterated upon until $Y = 0$ at $x = B$. Even though iteration is involved in solving Eq. (26), a simple iteration scheme can be written and the solution is readily obtained. This solution will be used to start the iteration process for the solution to the matrix equation, Eq. (17).

Results

In this section we will present some results for cones and for a blunt cone-cylinder. Comparisons are made for cavity shapes behind a cone and the cone drag with either more exact calculations or with experiments. For the blunt cone-cylinder, we will show the pressure distribution on the forebody and the cavity shapes for various cavitation and Froude numbers, including negative cavitation numbers.

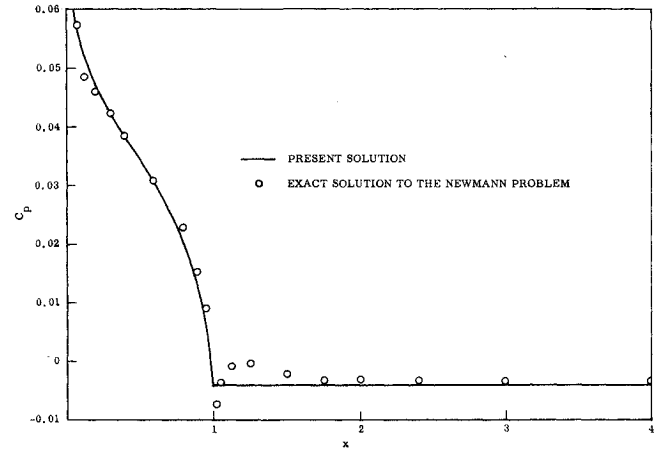

Fig. 3 Pressure distribution for a 5° cone at $\sigma = 0.0042$, $F \to \infty$.

Cone

The equation for a cone is, simply,

$$R_b = x \tan\theta \tag{27}$$

where θ is the half cone angle. From Eq. (27) we can calculate $\mathcal{L}(x)$ and $Y_b'(0)$ which will be needed in Eq. (18). Obviously, for the present point cone case, $Y_b'(0)$ is zero.

The results for a cone are plotted in Figs. 2–6. Figure 2 shows the cavity shape for a 5° cone at $\sigma = 0.0042$ and with no gravity effect ($F^2 \to \infty$). The shape is compared with that of Ref. 3. We see that they are in excellent agreement. Also shown in Fig. 2 is the cavity shape based on the approximate solution [solution to Eq. (26)]. It is seen that the approximate solution agrees closely near the cavity separation region (up to about $x = 2$). However, it deviates significantly from the more exact solution near the rear end of the cavity.

The pressure coefficient is plotted in Fig. 3. Also shown in this figure is the exact solution† to the so-called Neumann problem (dotted line). This is the solution to the potential flow over the body-cavity by considering the cavity as a solid boundary. The cavity shape used for the Neumann problem is provided by the present solution. Should the cavity shape given by the present solution be exact, the pressure coefficient on the cavity based on the Neumann solution should be constant and equal to the negative cavitation number. As we can see from Fig. 3, the pressure coefficient given by the present solution agrees very well with the exact Neumann solution, and on the cavity, the Neumann solution yields a pressure coefficient nearly constant and equal to negative cavitation numbers except near the cone base. In that region, the pressure coefficient oscillates. The poor agreement near the cone base is probably due to the fact that the present method of solution (by distributing singularities on axis of symmetry) cannot reproduce the curvature discontinuity at the body cavity junction.

†The author is indebted to J. A. Brosseau of Lockheed Missiles Space Co. Inc., for this exact solution to the Neumann problem.

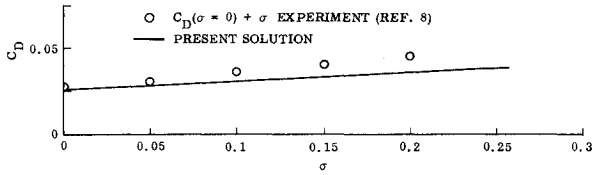

Fig. 5 Drag coefficient vs cavitation number for a 5° cone. $F \to \infty$.

Figure 4 shows the fineness ratio vs σ for 5° and 10° cone. The fineness ratio is defined as the ratio of the maximum diameter of the cavity d_{max} to the cavity length B-1. Comparisons are made with that of Ref. 3 and with the experimental data by Reichardt (taken from Ref. 8). The agreement is excellent.

The drag coefficient is plotted in Fig. 5 for a 5° cone at various σ. Also presented in this figure is the experimental data given in Ref. 9. It is seen that the present result becomes increasingly less accurate as the cavitation number increases. As we have indicated before, in order to apply the slender body theory σ must be order of $\delta^2 \ln \delta$. Therefore, as σ increases, the present solution becomes less valid.

The results we presented up to now are all gravity free. In order to see the gravity effect, we present, in Fig. 6, the pressure coefficients and the cavity shapes for several Froude numbers. The forebody shape for these cases is, again, a 5° cone. We see that the gravity effects are to reduce the cavity length and to reduce the pressure coefficient on the forebody. The gravity, therefore, seems to provide a mechanism for the closure of the cavity. The pressure coefficient is reduced because of buoyancy. For low speed, or for low Froude numbers, one can expect negative drag coefficients as shown in the case of $F^2 = 10$. We should note, however, that slender body theories will probably cease to be valid for such low Froude numbers.

Blunt Cone-Cylinder

We will present here some sample computations for a blunt cone-cylinder. This body shape is given by the following equations:

$$R_b^2 = 0.0498 \times -0.067x^2 \qquad 0 \leq x \leq 0.372$$

$$R_b^2 = 0.0093 \qquad 0.372 \leq x \leq 1 \qquad (28)$$

The results of these computations are plotted in Fig. 7 and Fig. 8. In Fig. 7, the cavity shapes for various F^2 and

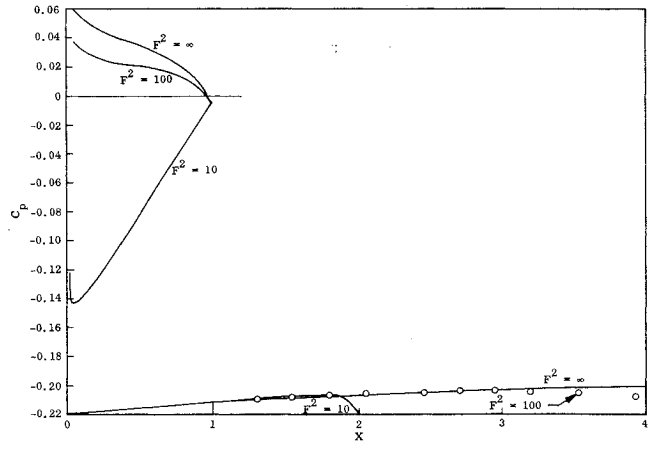

Fig. 6 Pressure distributions and cavity shapes for a 5° cone at various Froude numbers. $\sigma = 0.0042$.

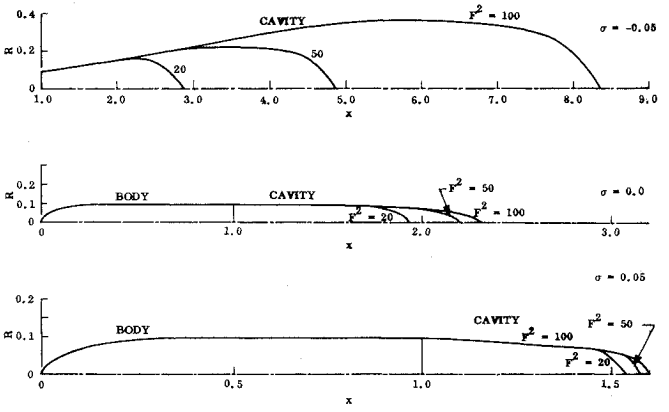

Fig. 7 Cavity shapes for a blunt cone-cylinder.

σ are given. It is seen that both the cavity shape and the cavity length depend strongly on cavitation number σ. For negative σ, the maximum diameter of the cavity is larger than the body base diameter and the cavity length is controlled by the Froude number. For zero or positive σ, the maximum diameter of the cavity is always less than that of the body base. The length of the cavity is influenced by the Froude number, but the influence is small for the large positive σ case. Indeed, for the case of $\sigma = 0.05$, the cavity lengths change very little for the three Froude numbers presently presented. Furthermore, the shapes are practically the same except near the rear end of the cavity. Hence, we can draw the following conclusion based on Fig. 7: for the blunt cone-cylinder, the gravity effect on the cavity shape seems to be small when the cavitation number is positive. By comparing Fig. 7 with Fig. 6, we see that the gravity effect on the cavity length is larger for a cone than for a blunt cone-cylinder. The degree of influence of gravity on the cavity shape is perhaps dependent on the cavity slope at the separation point.

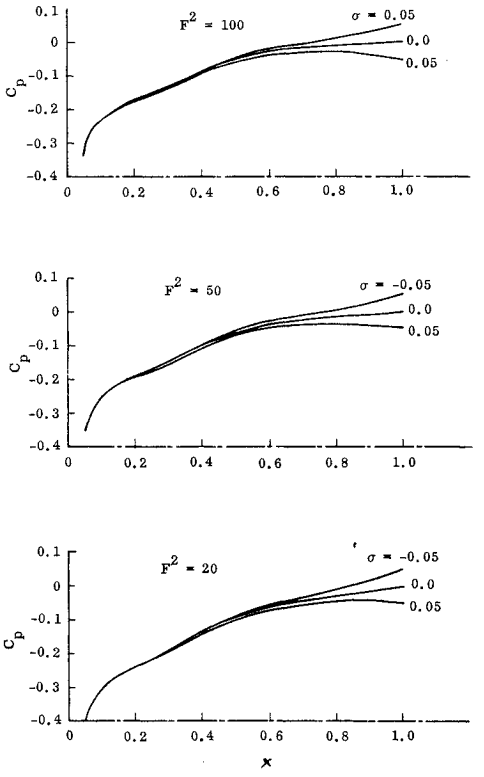

Fig. 8 Pressure distributions on a blunt cone-cylinder for various cavitation and Froude numbers.

Figure 8 shows the pressure coefficient on the forebody for various σ and F^2. For the cases presented, the body experiences buoyancy rather than drag since the pressure coefficients are mostly negative. From this figure, we see that the effect of cavitation number on pressure coefficient can be felt up to about 40% of the forebody length from the base.

Conclusions

A slender body theory has been applied to solve the axisymmetric supercavitating flows. Since the unknown cavity shape is determined by the constant pressure condition and the Bernoulli equation, the validity of the present solution depends not only on the slenderness δ being small, but also on the cavitation number σ being small and on the Froude number being large. Specifically, the solution will not be valid unless σ and $1/F^2$ are of the order of $\delta^2 \ln \delta$ or less.

The effects of the cavitation number and the Froude number on the cavity and forebody pressure coefficient have been studied. For zero or negative σ, the cavity cannot be closed unless gravity (acting in the positive x-direction) is present. In this case, the cavity length depends strongly on the Froude number, the smaller the F, the shorter the cavity. For positive σ, the cavity length is more sensitive to σ than to F. The effect of increasing σ on cavity length is to decrease it. In the case of a blunt cone-cylinder, the maximum diameter of the cavity is always less than the body base diameter for zero or positive σ; for negative σ with gravity, it is always larger than the body base diameter. The effect of gravity on cavity shape for positive σ is small.

To increase σ is to decrease the forebody pressure coefficient. In the case of a blunt cone-cylinder, the effect of varying σ on pressure coefficient can be felt about 40% of the forebody length from the base. To decrease F is to decrease the forebody pressure coefficient, the effect of varying F on pressure can be felt, obviously, throughout the entire forebody length.

The approximate solution given by Eq. (26) is an excellent first guess solution. A few iterations upon this solution lead to a converged solution to the integral equation.

References

[1]Gilbarg, D., "Jets and Cavities," *Encyclopedia of Physics,* Vol. IX, Fluid Dynamics III, Springer-Verlag, Berlin, 1960.

[2]Brennen, C., "A Numerical Solution of Axisymmetric Cavity Flows," *Journal of Fluid Mechanics,* Vol. 37, Pt. 4, 1969, pp. 671–688.

[3]Cuthbert, J. and Street, R., "An Approximate Theory for Supercavitating Flow About Slender Bodies of Revolution," LMSC Rept. TM81-73/39, Sept. 1964, Lockheed Missiles and Space Co., Sunnyvale, Calif.

[4]Struck, H. G., "Discontinuous Flows and Free Streamline Solutions for Axisymmetric Bodies at Zero and Small Angle of Attack," TND-5634 Feb. 1970, NASA.

[5]Laitone, E. V., "The Subsonic Flow About A Body of Revolution," *Quarterly of Applied Mathematics,* Vol. 5, 1947, pp. 227–231.

[6]Sears, W. R., *Small Perturbation Theory,* Princeton University Press, Princeton, N.J., 1960.

[7]Cumberbatch, E. and Wu, T. Y., "Cavity Flow Past A Slender Pointed Hydrofoil," *Journal of Fluid Mechanics,* Vol. 11, Pt. 2, 1961, pp. 187–208.

[8]Tulin, M. P., "Supercavitating Flow Past Foils and Struts," Chapter 16, *Symposium on Cavitation in Hydrodynamics,* National Physical Laboratory, Teddington, England, 1955.

[9]Cox, R. N. and Maceoll, J. W., "Recent Contribution to Basic Hydroballistics," *Symposium on Naval Hydrodynamics,* NAS-NRC Pub. 515, NASA, Washington, D.C., Chap. IX.